Relief of spin frustration through magnetic anisotropy in the quasi-one-dimensional $S = \frac{1}{2}$ antiferromagnet $Na_2CuSO_4Cl_2$

M. Fujihala,[1,*] Y. Sakuma,[1] S. Mitsuda,[1] A. Nakao,[2] K. Munakata,[2] R. A. Mole,[3] S. Yano,[4] D. H. Yu,[3] K. Takehana,[5] Y. Imanaka,[5] M. Akaki,[6] S. Okubo,[6] and H. Ohta[6]

[1]*Department of Physics, Faculty of Science, Tokyo University of Science, Shinjuku, Tokyo 162-8601, Japan*
[2]*Comprehensive Research Organization for Science and Society, Tokai, Ibaraki 319-1106, Japan*
[3]*Australian Nuclear Science and Technology Organisation, Lucas Heights, New South Wales 2232, Australia*
[4]*National Synchrotron Radiation Research Center, Neutron Group, Hsinchu 30077, Taiwan*
[5]*National Institute for Materials Science, 3-13 Sakura, Tsukuba, Ibaraki 305-0003, Japan*
[6]*Molecular Photoscience Research Center, Kobe University, 1-1 Rokkodai, Nada, Kobe, Hyogo 657-8501, Japan*

(Received 7 December 2021; revised 2 March 2022; accepted 29 March 2022; published 11 April 2022)

We report the magnetic structure and anisotropy of the quasi-one-dimensional $S = \frac{1}{2}$ antiferromagnet $Na_2CuSO_4Cl_2$ obtained by single-crystal neutron scattering, electron spin resonance (ESR), and magnetization measurements, following an earlier study of its dynamics [M. Fujihala *et al.*, Phys. Rev. B **101**, 024410 (2020)]. A Néel-type spin structure is formed within the chain of this compound, where the spins point along the *b* axis, and ESR data indicate an antisymmetric exchange with a uniform Dzyaloshinskii-Moriya (DM) vector pointing along the *b* axis. The anisotropy *g* factor and magnetic structure are strong indicators of magnetic anisotropy originating from a symmetric anisotropic exchange interaction and/or a magnetic dipole interaction. These results suggest that these terms of the anisotropic spin Hamiltonian counteract the effect of the DM interaction and stabilize the Néel-type structure in $Na_2CuSO_4Cl_2$.

DOI: 10.1103/PhysRevB.105.144410

I. INTRODUCTION

Considerable experimental and theoretical research has been devoted to studying frustrated low-dimensional magnets, which is one of the most important subjects in condensed-matter physics. In most magnets, three-dimensional (3D) coupling will induce magnetic ordering at finite temperatures. More to the point, the coexistence of such coupling and magnetic anisotropy stabilizes the 3D spin structure in low-dimensional spin systems. Therefore, to identify quantum phases, it is usually important to explore a model compound with negligibly small interchain or interlayer couplings. Although it is rare, a moderately strong interchain interaction can play an important role in quasi-one-dimensional (quasi-1D) spin systems with a uniform Dzyaloshinskii-Moriya (DM) interaction in realizing an exotic spin state [1,2]. The $S = \frac{1}{2}$ quasi-1D antiferromagnet $K_2CuSO_4X_2$ (X = Cl, Br) exhibits peculiar DM interactions that are uniform along its spin chains and antiparallel with respect to neighboring chains [3–7]. Linear spin chains along the *a* axis are formed by the exchange interaction through the Cu-Cl(Br)-Cl(Br)-Cu path, which is much larger than the interchain interactions [3]. Based on their crystal structure, $K_2CuSO_4X_2$ compounds exhibit substantial DM interactions that are aligned parallel to the *b* axis, as shown in Fig. 1. However, the DM vector is aligned antiparallel between adjacent chains. In this case, helical correlations with opposing helicity are present when interacting spin chains feature peculiar DM interactions that are uniform along the chain and antiparallel with respect to neighboring chains, thus resulting in unique spin frustration.

Recently, we reported the magnetic behaviors of $Na_2CuSO_4Cl_2$ [8], which possesses an orthorhombic crystal structure identical to $K_2CuSO_4X_2$. An inelastic neutron scattering (INS) study demonstrated that the quantum state of the 1D spin-$\frac{1}{2}$ Heisenberg antiferromagnet, which was previously revealed for $K_2CuSO_4X_2$, also exists in $Na_2CuSO_4Cl_2$. Linear spin chains along the *a* axis are formed by the exchange interaction $J_{Na} = 14.2$ K through the Cu-Cl-Cl-Cu path in $Na_2CuSO_4Cl_2$ (Fig. 1). An antiferromagnetic transition at $T_N = 0.54$ K was identified by specific heat and muon-spin rotation and relaxation (μSR) measurements. The ratio of the Néel temperature T_N to the intrachain interaction is 0.034 for $Na_2CuSO_4Cl_2$, which is close to that of $K_2CuSO_4Cl_2$ [3]. To understand the DM-induced frustration effects in 1D quantum spin systems, a systematic study of the spin dynamics and magnetic structure of the $A_2CuSO_4X_2$ (A = Na, K and X = Cl, Br) series is important, because the magnetic ground state is controlled by the magnitude relation between the interchain and DM interactions. Here, we report additional studies of $Na_2CuSO_4Cl_2$, focusing on the magnetic structure and magnetic anisotropy as investigated by single-crystal neutron scattering, electron spin resonance (ESR), and magnetization measurements.

II. EXPERIMENTAL DETAILS

Neutron-diffraction measurements were performed using the cold-neutron triple-axis spectrometer, Sika, installed at

*fujihara@nsmsmac4.ph.kagu.tus.ac.jp

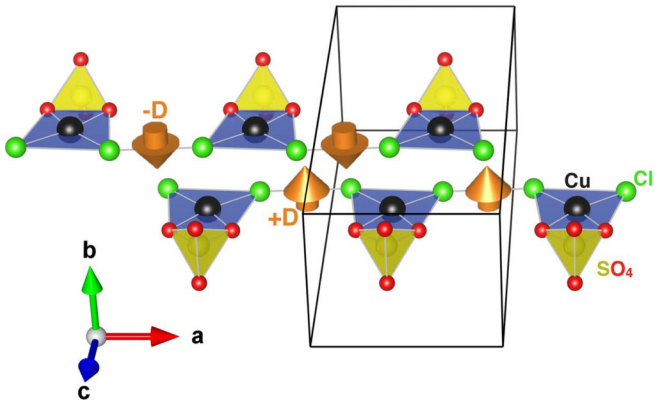

FIG. 1. The crystal structure of $Na_2CuSO_4Cl_2$. The Cu^{2+} ions (black) displayed with nearby oxygen (red), SO_4 ions (yellow tetrahedra), and chlorine ions (green). The direction of the Dzyaloshinskii-Moriya vector **D**, as determined by ESR measurements, is indicated by the orange arrow.

the Open Pool Australian Lightwater (OPAL) reactor at the Australian Nuclear Science and Technology Organisation [9]. Neutron-diffraction measurements in a wide reciprocal space were performed using a time-of-flight (TOF) neutron diffractometer (BL18 SENJU) installed at the Materials and Life Science Experimental Facility (MLF) of the Japan Proton Accelerator Research Complex (J-PARC) [10]. The collected data were processed with the software STARGAZER [11]. The INS experiments were performed using the cold-neutron TOF spectrometer Pelican at the OPAL reactor at ANSTO [12]. The instrument was aligned for an incident energy of $E_i = 3.68$ meV. The sample employed in the experiment at Sika and Pelican was held in an oxygen-free copper can and cooled using a dilution insert installed in a top-loading cryostat. The sample data were corrected for background scattering from the empty dilution insert and normalized to the scattering from a vanadium standard. The data were processed using a combination of the freely available MANTID software [13]. High-field multifrequency ESR measurements were performed using pulsed magnetic fields up to 13 T in the frequency range from 70 to 260 GHz at several temperatures. A standard of 2,2-diphenyl-1-picrylhydrazyl (known as DPPH) was employed as a $g = 2.0036$ marker for the magnetic field. Low-field magnetization measurements were performed using a commercial superconducting quantum interference device magnetometer (MPMS-XL7AC: Quantum Design). The high-field magnetization was carried out by an extraction method with a 15-T superconducting magnet installed at the Tsukuba Magnet Laboratory in the National Institute for Materials Science. The crystal and magnetic structure were visualized using the VESTA software [14].

III. RESULTS AND DISCUSSION

Figures 2(a)–2(c) show the contour map of the neutron intensity at $T = 3$ and 0.3 K in the $(hk0)$ plane at the first frame. The nuclear Bragg peaks are indexed by the orthorhombic unit cell with $a = 6.9875(2)$ Å, $b = 5.5657(2)$ Å, and $c = 15.9716(5)$ Å, and there is no structural transition in $Na_2CuSO_4Cl_2$ around $T_N = 0.54$ K [8]. Below T_N, about 100 magnetic reflection peaks were observed on the $(\frac{n}{2}kl)$ where n is an odd integer. The inset of Fig. 2(d) shows the peak profiles of the 0.5 0 0 magnetic peak along the TOF direction at several temperatures. The integrated intensity decreases with increasing temperature and then disappears above 0.54 K (see Supplemental Material Fig. S2) [15], consistent with our previous study. Analyzing the intensity with the power law,

$$I_{0.500} \propto \left(\frac{T_N - T}{T_N}\right)^{2\beta}, \tag{1}$$

yields the critical exponent $\beta \approx 0.17$. The value of β is different from the critical exponent expected for a 3D magnetic system ($\beta = 0.36$). This behavior is also observed in our previous μSR study [8].

The presence of the $(\frac{n}{2}kl)$ magnetic peaks indicates that nearest-neighbor Cu atoms within a chain have exactly antiparallel magnetic moments and the magnetic unit cell is twice as large as a chemical unit cell along the a axis. Four magnetic Cu^{2+} ions are located on the Wyckoff positions $4c$: $\mathbf{r}_1 = (0.636, 0.25, 0.966)$, $\mathbf{r}_2 = (0.136, 0.25, 0.534)$, $\mathbf{r}_3 = (0.364, 0.75, 0.034)$, and $\mathbf{r}_4 = (0.864, 0.75, 0.466)$ in the orthorhombic unit cell with space group *Pnma*. In this case, the possible magnetic structure can be represented by only four irreducible spin arrangements $(\uparrow, \uparrow, \uparrow, \uparrow)$, $(\downarrow, \uparrow, \uparrow, \uparrow)$, $(\uparrow, \downarrow, \uparrow, \uparrow)$, and $(\downarrow, \downarrow, \uparrow, \uparrow)$, where the parentheses show the relative phase factors of the spins on the sites $(\mathbf{r}_1, \mathbf{r}_2, \mathbf{r}_3, \mathbf{r}_4)$ [16]. Therefore, in the case that the spins are pointing along one of the crystal axes, there are only 12 possible magnetic structures.

Figure 3(a) shows the observed intensities I_{obs}^{Nuc} and I_{obs}^{Mag} plotted against calculated intensities I_{calc}^{Nuc} and I_{calc}^{Mag} for the nuclear and magnetic peaks. The I_{calc}^{Mag} presented in Fig. 3(a) are calculated for the magnetic structure shown in Fig. 3(b). The intensities of the nuclear scattering I_{calc}^{Nuc} are obtained by

$$I_{calc}^{Nuc} = |F_{Nuc}|^2 \frac{\lambda^4}{\sin^2\theta}, \tag{2}$$

where F_{Nuc} is the nuclear structure factor simulated using the RIETAN-FP software [17]. The intensities of the magnetic scattering I_{calc}^{Mag} are obtained by

$$I_{calc}^{Mag} = |F_{Mag}|^2 \frac{\lambda^4}{\sin^2\theta}, \tag{3}$$

$$F_{Mag} = \sum_i f_i(\mathbf{Q}) \mu_{\perp i} \exp\{2\pi\, i(\mathbf{Q} \cdot \mathbf{r}_i + \phi_i)\}, \tag{4}$$

where F_{Mag}, λ, θ, $f_i(\mathbf{Q})$, $\mu_{\perp i}$, and ϕ_i represent the magnetic structure factor, wavelength of neutrons, scattering angle divided by 2, magnetic form factor [18], component of the ordered moment of Cu^{2+} ion perpendicular to $\mathbf{Q}$, and the relative phase shift at the $\mathbf{r}_i$ ($\phi_i = 0$ or π), respectively. $\frac{\lambda^4}{\sin^2\theta}$ is the Lorentz factor for the TOF diffractometer. In general, the extinction effect weakens the peak intensity in the higher intensity region. In fact, as shown in Fig. 3(a), the intensities of the nuclear scattering deviate gradually from the straight line. On the other hand, the intensities of the magnetic scattering seem to not be affected by this. Based on the goodness of fit, a candidate magnetic structure is obtained, as shown in Fig. 3(b) (see Supplemental Material for details [15]). There is no large

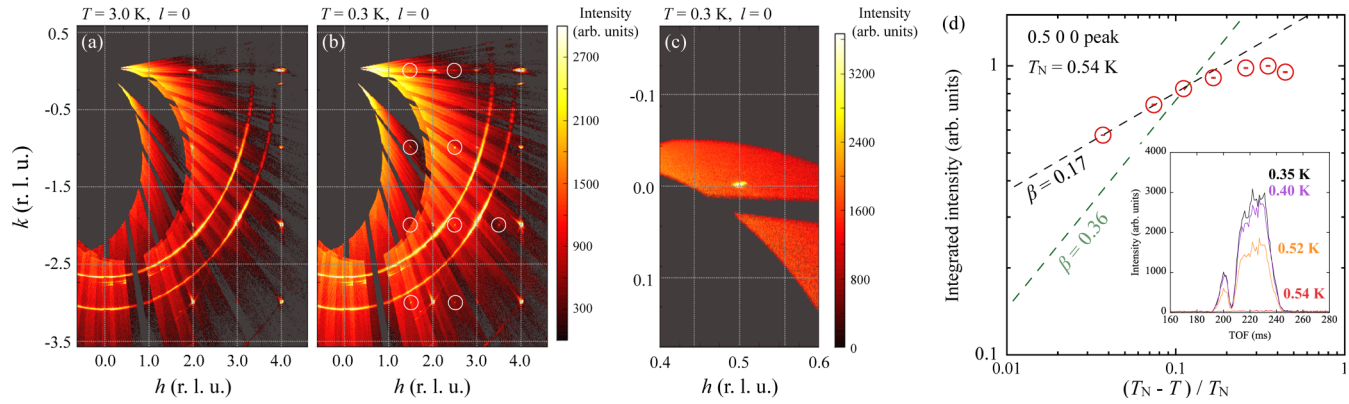

FIG. 2. Contour map of neutron intensity in the ($hk0$) plane at (a) $T = 3$ K and (b) $T = 0.3$ K. The magnetic peak is indicated by the white circles. (c) Contour map of neutron intensity in the ($hk0$) plane around the reciprocal lattice point 0.5 0 0 at $T = 0.3$ K. (d) Temperature dependence of the intensity of the 0.5 0 0 magnetic peak for $Na_2CuSO_4Cl_2$ (open red circles). The dashed lines show power-law fits. The inset shows the peak profiles of the 0.5 0 0 magnetic peak along the TOF direction at several temperatures.

deviation between the calculated magnetic intensities with $\mu_i = 1\mu_B$ and the line fitted to the observed nuclear intensity in the almost extinction-free region [Fig. 3(a)], indicating that the ordered moment has a value which is close to that for the expected full moment for a spin $\frac{1}{2}$. The spin direction is parallel to the DM vector expected from the crystal structure, indicating that the DM interaction is not the driving force for the magnetic phase transition.

The magnetic excitation spectra measured at 0.7 K and 50 mK have the features of a 1D $S = \frac{1}{2}$ Heisenberg antiferromagnet. As shown in Fig. 4(a), the spectrum measured at 50 mK is in qualitative agreement with previous results measured at 1.5 K. The spinon continuum edges rise from the Brillouin zone centers in the chain direction. In addition, the observed lower-energy boundary of the continuum is con-

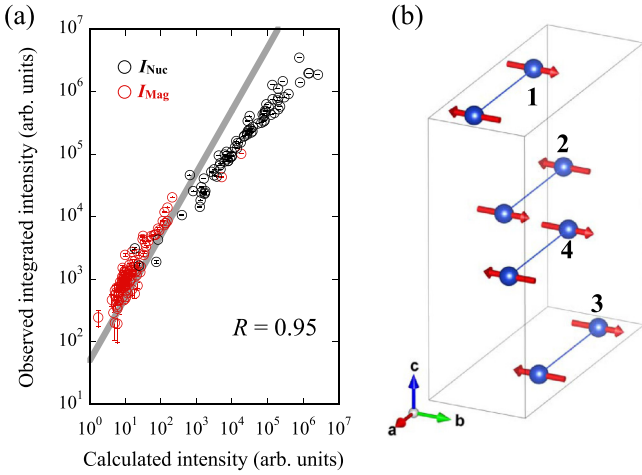

FIG. 3. (a) Observed intensities of the nuclear and magnetic scattering plotted against calculated values for the nuclear and magnetic peaks. The intensities of the magnetic scattering are calculated for the magnetic structure shown in (b). The solid gray line is a linear fit to the observed nuclear intensities below 1000 intensity units. The values in the plot show the obtained ordered moment and Pearson's correlation coefficient R. (b) Possible magnetic structure of $Na_2CuSO_4Cl_2$. The thick black lines show the magnetic unit cell. The Cu^{2+} positions are labeled 1–4 according to their positions $\mathbf{r}_1$–$\mathbf{r}_4$.

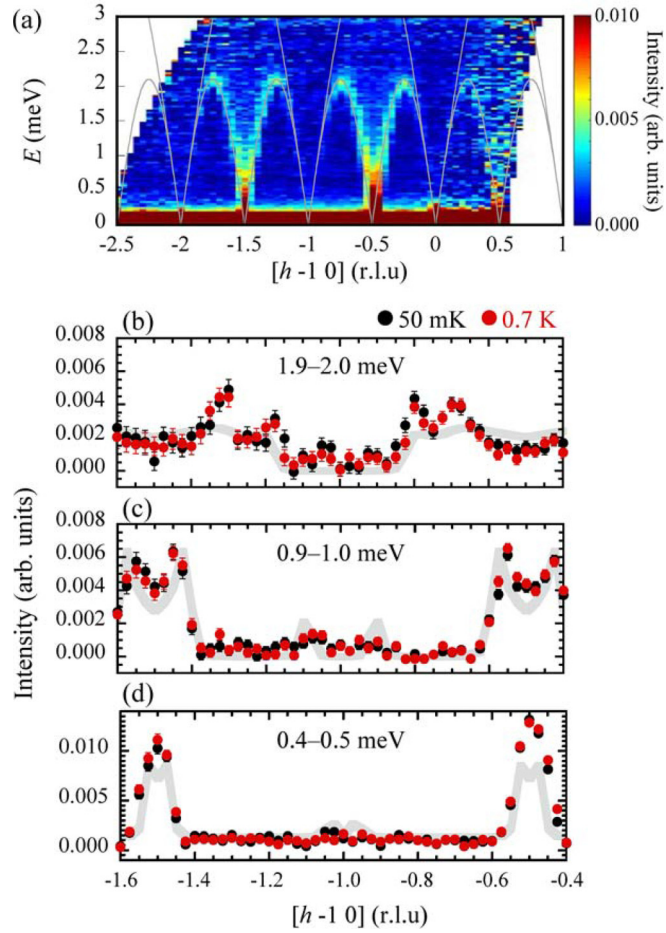

FIG. 4. (a) INS spectrum along the a axis of $Na_2CuSO_4Cl_2$ measured at 50 mK with an incident neutron energy of 3.68 meV. The intensities were integrated over k from -3 to 1 and l from -1 to 1. The superimposed gray solid lines indicate the lower and upper energy boundaries of the continuum given by $(\pi J_{Na}/2)|\sin(\pi h)|$ and $\pi J_{Na}|\sin(\pi h/2)|$ [21]. (b)–(d) Constant-E cuts of the measured scattering intensity at above and below T_N (50 mK and 0.7 K). The intensity in each panel is integrated within the energy range shown in the upper center. The gray thick lines are fits using the approximate, semiempirical Müller ansatz expression [see Eq. (4) in Ref. [19]].

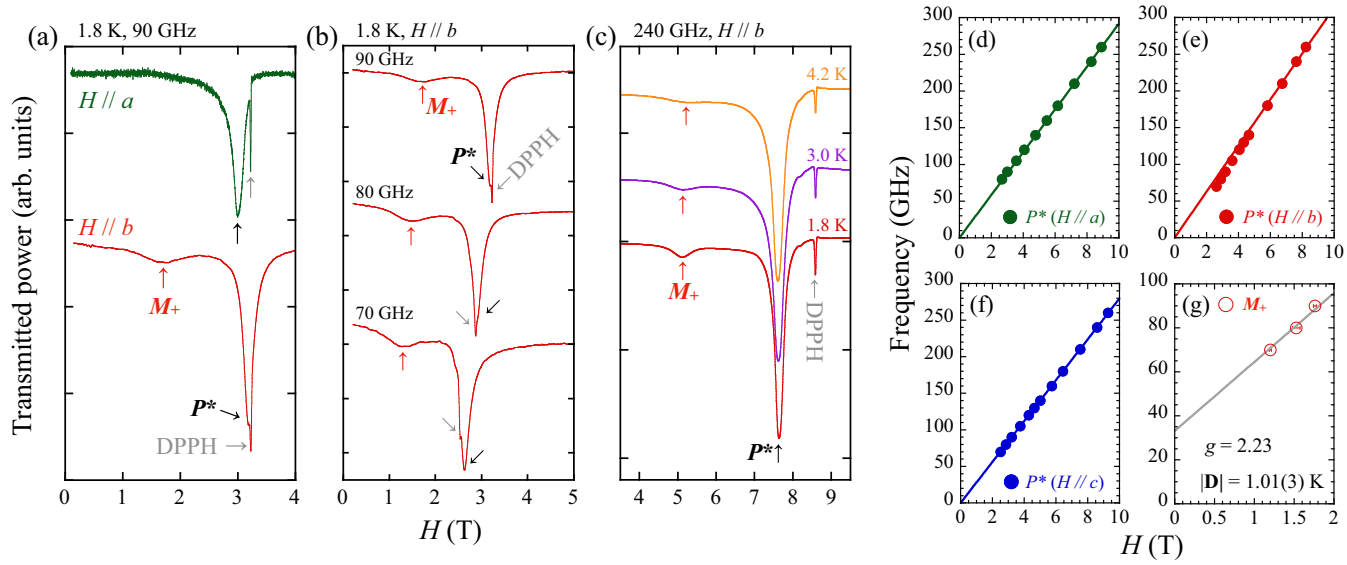

FIG. 5. (a) ESR spectra of $Na_2CuSO_4Cl_2$ at 1.8 K with a magnetic field applied along the a axis and b axis. The red arrows mark mode M_+. The black arrows mark the paramagnetic mode P^*. The narrow peaks marked by gray arrows are the mode DPPH. (b) ESR spectra for a magnetic field parallel to the DM vector ($H \parallel b$) for various frequencies. (c) Temperature evolution of the 240 GHz ESR spectra at $H \parallel b$. Frequency-field diagrams of mode P^* for (d) $H \parallel a$, (e) $H \parallel b$, (f) $H \parallel c$ at $T = 1.8$ K. The solid lines show the Larmor frequency $\nu = g\mu_B H/(2\pi\hbar)$. (g) Frequency-field diagram of mode M_+ at $T = 1.8$ K. The gray line behind the data points denotes the fitting curves by Eq. (7).

sistent with the theoretical line for a 1D spin-$\frac{1}{2}$ Heisenberg antiferromagnet given by $(\pi J_{\rm Na} d/2)|\sin(2\pi h)|$. The continuum is reflected in the dynamical structure factor probed by INS, and the constant-energy (constant-E) cuts can be described by the approximate, semiempirical Müller ansatz equation [19,20]. As shown in Figs. 4(b)–4(d), these results of fitting the equation to the data are reasonably good. No significant changes were observed above and below $T_{\rm N}$, at least within the instrumental resolution. It is clear that the spinon continuum is observed even below $T_{\rm N}$, where long-range magnetic order develops. Such excitation is often observed in quasi-1D spin-$\frac{1}{2}$ Heisenberg antiferromagnets where the interchain interaction is relatively small [21].

ESR is a sensitive probe for DM interactions in spin chain systems. Considering a single Heisenberg chain with a uniform DM interaction, theory suggests that the spinon spectrum is shifted by $q = |\mathbf{D}|/Jd$ (d is the distance between nearest-neighbor spins), which causes the splitting of the ESR mode at the gamma point [22]. In the case of $\mathbf{D} \parallel b$, at zero temperature, the theoretical analysis predicted the two following resonance frequencies [4,23]:

$$(2\pi\nu_+)^2 = (g_a\mu_B H_a)^2 + (g_b\mu_B H_b + \pi|\mathbf{D}|/2)^2 + (g_c\mu_B \mathrm{H_c})^2, \tag{5}$$

$$(2\pi\nu_-)^2 = (g_a\mu_B H_a)^2 + (g_b\mu_B H_b - \pi|\mathbf{D}|/2)^2 + (g_c\mu_B \mathrm{H_c})^2. \tag{6}$$

In the limiting cases of $H \parallel \mathbf{D}$ and $H \perp \mathbf{D}$ these equations correspondingly transform into

$$\nu_\pm = \frac{1}{2\pi\hbar}\left|g_b\mu_B H \pm \frac{\pi}{2}|\mathbf{D}|\right|, \tag{7}$$

$$\nu_\perp = \frac{1}{2\pi\hbar}\sqrt{(g_\perp\mu_B H)^2 + \left(\frac{\pi}{2}|\mathbf{D}|\right)^2}. \tag{8}$$

Here, $g_\perp$ is the value of g factor for the field oriented perpendicular to b. In fact, the ESR doublet M_+ and M_- is clearly observed below $T = 20.4$ K at $H \parallel b$ in $K_2CuSO_4Br_2$ [4]. As shown in Fig. 5(a), a single absorption line, labeled as P^*, is observed for a field applied along the a axis. The single Lorentzian ESR absorption line clearly observed in the high-frequency region is typical paramagnetic resonance. In contrast, two lines (P^* and M_+) are clearly observed at temperature 1.8 K and frequency $\nu = 90$ GHz for a field along the b axis. The P^* absorption for a field applied along the b axis appears to be asymmetrical in the low-frequency region, suggesting that it is a sum of two components P^* and M_- [Fig. 5(b)]. In fact, as shown Fig. 5(e), the frequency dependence of the resonance fields deviates from the straight line in the low-frequency region. The resonance fields of modes M_+ and M_- should be equidistant to the left and right of the main line P^*, respectively, according to Eq. (7). However, the asymmetric temperature dependencies of the resonance fields of modes M_+ and M_- were observed in $K_2CuSO_4Br_2$ [4]. In the temperature range of $T > |\mathbf{D}|$, depending on the frequency range that can be measured, it becomes difficult to separate the P^* and M_- lines. The temperature evolution of the 240-GHz ESR line at $H \parallel b$ is shown in Fig. 5(c), showing that M_+ develops with decreasing temperature. These results indicate an antisymmetric exchange with a uniform DM vector pointing along the b axis, as shown in Fig. 1.

Figures 5(d)–5(f) show the frequency-field diagram for ESR at 1.8 K for a field applied along the a, b, and c axes, respectively. For frequencies above 150 GHz the doublet declines considerably and a strong Lorentzian ESR absorption line with the paramagnetic resonance frequency $\nu = g\mu_B H/(2\pi\hbar)$ is observed. The values of the g factor are estimated to be $g_a = 2.07(1)$, $g_b = 2.23(2)$, and $g_c = 1.99(1)$, respectively.

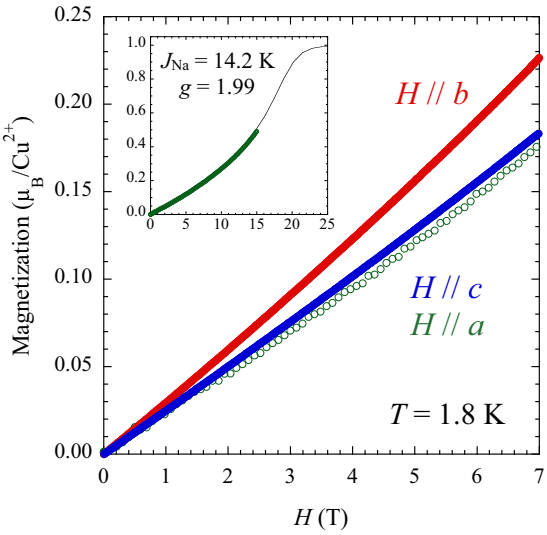

FIG. 6. Magnetization curves of $Na_2CuSO_4Cl_2$ measured down to 1.8 K and up to 7 T along the a (open green circles), b (solid red circles), and c axes (solid blue circles). The inset shows the magnetization curve measured using the extraction method down to 1.8 K and up to 15 T along the a axis. The solid line shows theoretical data computed by the quantum Monte Carlo method for a linear spin chain model at the temperatures used in the experiments with $J_{Na} = 14.3$ K and $g = 1.99$.

In the case that $2\pi\hbar\nu$ is much smaller than J_{Na} and a magnetic field is applied along **D**, ESR resonances are observed at the frequencies $\nu_{\pm}$. We could not separate the intensity of the modes P^* and M_- from the data for a field applied along b; however, the resonance fields of mode M_+ can be determined. The value of $|\mathbf{D}|$ is estimated to be 1.01(3) K by fitting the frequency dependencies of the resonance fields of mode M_+ with $\frac{1}{2\pi\hbar} g_b \mu_B H + \frac{\pi}{2}|\mathbf{D}|$. The estimated value is larger than the Néel temperature $T_N = 0.54$ K of $Na_2CuSO_4Cl_2$.

As shown in the inset in Fig. 6, a marked upturn curvature is observed in the magnetization curve measured at 1.8 K with the applied magnetic field along the a axis, indicating a 1D antiferromagnetic correlation. The magnetization of a linear-chain system for $J_{Na} = 14.3$ K and $g = 1.99$ is calculated by the quantum Monte Carlo method using the ALPS package [24]. The calculated result is in good agreement with the experimental data. As shown in Fig. 6, the anisotropy in the magnetization for $H \parallel a$, b, and c reflects the anisotropy in the g values.

Most low-dimensional copper salts exhibit long-range magnetic ordering at low temperature, with the spins pointing in a specific direction in the crystal, suggesting that there is a finite magnetic anisotropy in these salts. In copper salts, there is no anisotropy energy arising from the crystal field because Cu^{2+} ions have a spin of $\frac{1}{2}$, therefore, the specific spin structure in the magnetic ordered state is a result of the coinfluence of the magnetic dipole interaction, symmetric anisotropic exchange interaction, and DM interaction (antisymmetric anisotropic exchange) [25]. Unfortunately, it is not possible to estimate the magnitude of these anisotropies from the present experimental results. In $K_2CuSO_4X_2$, the DM interaction is considered as the dominant magnetic anisotropy term. The DM interaction mediates a spin-spin coupling of the form $\mathbf{D} \cdot (\mathbf{S}_1 \times \mathbf{S}_2)$, which is usually responsible for the helimagnetic spin arrangement in 1D spin chains. In contrast, a magnetic dipole interaction and symmetric anisotropic exchange interaction require the spins to point along a specific direction in the crystal, either parallel or antiparallel. The estimated g factors and magnetic structure of $Na_2CuSO_4Cl_2$ strongly suggest the presence of a magnetic dipole interaction and/or symmetric anisotropic exchange interaction. We consider that other terms in the anisotropic spin Hamiltonian counteract the effects of the DM interaction and stabilize the Néel-type structure in this system.

In summary, we have determined that the magnetic structure of $Na_2CuSO_4Cl_2$ is a simple Néel-type order along the b axis. $|\mathbf{D}|$ is estimated to be 1.01(3) K, which is larger than the Néel temperature $T_N = 0.54$ K of $Na_2CuSO_4Cl_2$. The anisotropy in the magnetization for $H \parallel a$, b, and c reflects the anisotropy in the g values. These results indicate that for $Na_2CuSO_4Cl_2$, other anisotropy terms must be added to the spin Hamiltonian in addition to the DM term. The other anisotropy terms contribute to relieving the DM-induced frustration, which should also occur in the other family compounds. Both the DM and intrachain interactions depend on the orbital overlap in the chains and are proportional to each other. In addition, the other anisotropies depend on the crystal structure. The structural similarity between the chains in $Na_2CuSO_4Cl_2$ and $K_2CuSO_4X_2$ suggests that the ratio of these effects may be similar. We believe it is important to find a different model compound to study the intrinsic magnetism on the unique frustration induced by DM interactions.

ACKNOWLEDGMENTS

The neutron scattering experiments were performed at the MLF (J-PARC) and OPAL reactor (ANSTO) under a user program (Proposals No. 2019A0106, No. P6517, and No. P6913). This study is supported by a Grant-in-Aid for Scientific Research (No. 21K03453 and No. 17K14344) from MEXT, Japan.

[1] M. Kargarian, R. Jafari, and A. Langari, Phys. Rev. A **79**, 042319 (2009).
[2] I. Garate and I. Affleck, Phys. Rev. B **81**, 144419 (2010).
[3] M. Hälg, W. E. A. Lorenz, K. Yu. Povarov, M. Månsson, Y. Skourski, and A. Zheludev, Phys. Rev. B **90**, 174413 (2014).
[4] A. I. Smirnov, T. A. Soldatov, K. Yu. Povarov, M. Hälg, W. E. A. Lorenz, and A. Zheludev, Phys. Rev. B **92**, 134417 (2015).
[5] D. Blosser, N. Kestin, K. Yu. Povarov, R. Bewley, E. Coira, T. Giamarchi, and A. Zheludev, Phys. Rev. B **96**, 134406 (2017).
[6] W. Jin and O. A. Starykh, Phys. Rev. B **95**, 214404 (2017).
[7] T. A. Soldatov, A. I. Smirnov, K. Yu. Povarov, M. Hälg, W. E. A. Lorenz, and A. Zheludev, Phys. Rev. B **98**, 144440 (2018).
[8] M. Fujihala, S. Mitsuda, R. A. Mole, D. H. Yu, I. Watanabe, S. Yano, T. Kuwai, H. Sagayama, T. Kouchi, H. Kamebuchi, and M. Tadokoro, Phys. Rev. B **101**, 024410 (2020).

[9] C.-M. Wu, G. Deng, J. S. Gardner, P. Vorderwisch, W.-H. Li, S. Yano, J.-C. Peng, and E. Imamovic, J. Instrum. **11**, P10009 (2016).
[10] T. Ohhara, R. Kiyanagi, K. Oikawa, K. Kaneko, T. Kawasaki, I. Tamura, A. Nakao, T. Hanashima, K. Munakata, T. Moyoshi, T. Kuroda, H. Kimura, T. Sakakura, C.-H. Lee, M. Takahashi, K.-I. Ohshima, T. Kiyotani, Y. Noda, and M. Arai, J. Appl. Crystallogr. **49**, 120 (2016).
[11] T. Ohhara, K. Kusaka, T. Hosoya, K. Kurihara, K. Tomoyori, N. Niimura, I. Tanaka, J. Suzuki, T. Nakatani, T. Otomo, S. Matsuoka, K. Tomita, Y. Nishimaki, T. Ajima, and S. Ryufuku, Nucl. Instrum. Methods Phys. Res., Sect. A **600**, 195 (2009).
[12] D. Yu, R. Mole, T. Noakes, S. Kennedy, and R. Robinson, J. Phys. Soc. Jpn. **82**, SA027 (2013).
[13] O. Arnold, J. C. Bilheux, J. M. Borreguero, A. Buts, S. I. Campbell, L. Chapon, M. Doucet, N. Draper, R. F. Leal, M. A. Gigg, V. E. Lynch, A. Markvardsen, D. J. Mikkelson, R. L. Mikkelson, R. Miller, K. Palmen, P. Parker, G. Passos, T. G. Perring, P. F. Peterson *et al.*, Nucl. Instrum. Methods Phys. Res., Sect. A **764**, 156 (2014).
[14] K. Momma and F. Izumi, J. Appl. Crystallogr. **44**, 1272 (2011).
[15] See Supplemental Material at http://link.aps.org/supplemental/10.1103/PhysRevB.105.144410 for the experimental details.
[16] R. Toft-Petersen, M. Reehuis, T. B. S. Jensen, N. H. Andersen, J. Li, M. D. Le, M. Laver, C. Niedermayer, B. Klemke, K. Lefmann, and D. Vaknin, Phys. Rev. B **92**, 024404 (2015).
[17] F. Izumi and K. Momma, Solid State Phenom. **130**, 15 (2007).
[18] S. W. Lovesey, *Theory of Neutron Scattering from Condensed Matter* (Oxford Science Publishers, Oxford, UK, 1984).
[19] G. Müller, H. Thomas, H. Beck, and J. C. Bonner, Phys. Rev. B **24**, 1429 (1981).
[20] I. A. Zaliznyak, H. Woo, T. G. Perring, C. L. Broholm, C. D. Frost, and H. Takagi, Phys. Rev. Lett. **93**, 087202 (2004).
[21] B. Lake, D. A. Tennant, C. D. Frost, and S. E. Nagler, Nat. Mater. **4**, 329 (2005).
[22] S. Gangadharaiah, J. Sun, and O. A. Starykh, Phys. Rev. B **78**, 054436 (2008).
[23] K. Y. Povarov, A. I. Smirnov, O. A. Starykh, S. V. Petrov, and A. Y. Shapiro, Phys. Rev. Lett. **107**, 037204 (2011).
[24] A. F. Albuquerque, F. Alet, P. Corboz, P. Dayal, A. Feiguin, S. Fuchs, L. Gamper, E. Gull, S. Gürtler, A. Honecker, R. Igarashi, M. Körner, A. Kozhevnikov, A. Läuchli, S. R. Manmana, M. Matsumoto, I. P. McCulloch, F. Michel, R. M. Noack, G. Pawłowski, L. Pollet, T. Pruschke, U. Schollwöck, S. Todo, S. Trebst *et al.*, J. Magn. Magn. Mater. **310**, 1187 (2007).
[25] T. Moriya and K. Yosida, Prog. Theor. Phys. **9**, 663 (1953).